Available online at www.sciencedirect.com
SCIENCE DIRECT®
Carbon xxx (2004) xxx–xxx
CARBON
www.elsevier.com/locate/carbon

Hydrophobic hydration of C_{60} and carbon nanotubes in water

J.H. Walther [a,*], R.L. Jaffe [c], E.M. Kotsalis [a], T. Werder [a], T. Halicioglu [b], P. Koumoutsakos [a]

[a] *Institute of Computational Science, Swiss Federal Institute of Technology, Hirschengraben 84, ETH Zürich CH-8092, Switzerland*
[b] *Eloret Corp., 690 W. Fremont Ave., Sunnyvale, CA 94087, USA*
[c] *NASA Ames Research Center, Moffett Field, CA 94035, USA*

Abstract

We perform molecular dynamics (MD) simulations to study the hydrophobic–hydrophilic behavior of pairs of C_{60} fullerene molecules and single wall carbon nanotubes in water. The interaction potentials involve a fully atomistic description of the fullerenes or carbon nanotubes and the water is modeled using the flexible SPC model. Both unconstrained and constrained MD simulations are carried out. We find that these systems display drying, as evidenced by expulsion of the interstitial water, when the C_{60} and carbon nanotubes are separated by less than 12, and 9–10 Å, respectively. From the constrained simulations, the computed mean force between two carbon nanotubes in water exhibits a maximum at a tube spacing of 5.0 Å which corresponds to approximately one unstable layer of interstitial water molecules. The main contribution to the force stems from the van der Waals attraction between the carbon surfaces. The minimum in the potential of mean force has a value of -17 kJ mol^{-1} Å^{-1} at a tube spacing of 3.5 Å.

Keywords: A. Carbon nanotube, Fullerene; C. Molecular simulations; D. Aggregation, Interfacial properties

1. Introduction

The applicability of carbon nanotubes (CNT) as sensory [1–3] and manipulating devices in biological systems [4,5] is critically related to their solubility and wettability in aqueous environments, or in general with their *hydrophobic–hydrophilic* behavior. Graphite is considered to be hydrophobic [6–9], and carbon nanotubes, which correspond to hollow cylinders of rolled-up graphene, and fullerenes are found to have a low solubility in water [10–14]. However, water is expected to wet and fill carbon nanotubes due to its relatively low surface tension [15]. Indeed partial wetting of capped multiwall carbon nanotubes was recently observed experimentally [16] in liquid inclusions composed of 85.2% water, 7.4% CO_2, and 7.4% CH_4, respectively. However, the observed wetting in these experiments was later found to be influenced by the presence of hydrophilic groups (e.g., –OH and –COOH) on the interior of the carbon nanotube [17]. In contrast, a non-wetting or hydrophobic behavior was found in numerical studies of pure water surrounding a pristine carbon nanotube [18], and water droplets inside carbon nanotubes were found to have a contact angle of 106° [19], indicative of a hydrophobic interface. Other recent simulations include studies of spontaneous filling of narrow carbon nanotubes [20], and the formation of helical ice structures [21] at physiological conditions (1 atm and 300 K) and at elevated pressures [22], indicating a hydrophilic-like behavior of the carbon nanotube interior. The drying of arrays of carbon nanotubes was recently observed during wet treatment and purification of aligned carbon nanotubes intended as a nanoelectrode platform for biosensor development [5]. Shortening the arrays by partially filling the gaps and covering the sidewalls of the carbon nanotubes with a spin-on glass resulted in a mechanically stable system.

In the present study, we consider as a canonical problem the hydrophobic–hydrophilic behavior of a pair of C_{60} molecules and two and 16 (16,0) carbon nanotubes surrounded by water at physiological conditions. These systems are modeled using fully atomistic molecular dynamics (MD) simulations. The C_{60} buckyballs and carbon nanotubes are described by Morse

* Corresponding author. Tel.: +41-1-632-2645; fax: +41-1-632-1703.
E-mail addresses: walther@inf.ethz.ch (J.H. Walther), rjaffe@mail.arc.nasa.gov (R.L. Jaffe), kotsalis@inf.ethz.ch (E.M. Kotsalis), werder@inf.ethz.ch (T. Werder), haliciog@nas.nasa.gov (T. Halicioglu), petros@inf.ethz.ch (P. Koumoutsakos).

0008-6223/$ - see front matter © 2004 Elsevier Ltd. All rights reserved.
doi:10.1016/j.carbon.2003.12.071

stretch, harmonic bend, torsion, and a carbon–carbon Lennard-Jones potential, and the water by the flexible SPC model of Teleman et al. [23]. The carbon–water interaction is described by a carbon–oxygen Lennard-Jones term. We consider the stability of the interstitial water molecules and derive the potential of mean force for the two carbon nanotubes in water. The results indicate that for physically realistic interaction potentials the dominant force aggregating the carbon nanotubes is the van der Waals attraction between the carbon nanotubes. Only purely repulsive carbon–water interactions result in a "long-range" hydrophobic hydration of the carbon nanotubes.

2. Molecular dynamics simulations

The carbon nanotube–water system is modeled using classical molecular dynamics simulations subject to periodic boundary conditions in two or three spatial directions, the former for the studies involving a free surface corresponding to carbon nanotubes immersed in a slab of water. The latter were carried out in an NVE ensemble. In all cases, temperature scaling is imposed only during the initial equilibration period.

The water intramolecular potential energy is described by the flexible SPC model [23] which features harmonic stretch and bend terms between the oxygen and hydrogen atoms. The water–water interaction is described by an oxygen–oxygen Lennard-Jones term and Coulomb terms between partial charges located on the hydrogen and oxygen atoms. The Coulomb interaction is computed using a smooth truncation [24] with a cutoff fixed for each case, at a value of 9.50–12.66 Å. The carbon nanotube energies are modeled by terms describing Morse bond, harmonic cosine of the bending angle, and a 2-fold torsion potential [18,25,26]

$$U(r_{ij},\theta_{ijk},\phi_{ijkl}) = K_{\mathrm{Cr}}(\xi_{ij}-1)^2 + \frac{1}{2}K_{\mathrm{C}\theta}(\cos\theta_{ijk}-\cos\theta_{\mathrm{C}})^2 + \frac{1}{2}K_{\mathrm{C}\phi}(1-\cos 2\phi_{ijkl}), \quad (1)$$

where

$$\xi_{ij} = \mathrm{e}^{-\gamma(r_{ij}-r_{\mathrm{C}})}, \quad (2)$$

and θ_{ijk} and ϕ_{ijkl} represent all the possible bending and torsion angles, and r_{ij} represents all the distances between bonded atoms. K_{C}, $K_{\mathrm{C}\theta}$ and $K_{\mathrm{C}\phi}$ are the force constants of the stretch, bend and torsion potentials, respectively, and r_{C}, θ_{C}, and ϕ_{C} the corresponding reference geometry parameters for graphene. A pairwise Lennard-Jones term is added to the nanotube potential to account for the steric and van der Waals carbon–carbon interaction

$$U(r_{ij}) = 4\epsilon_{\mathrm{CC}}\left[\left(\frac{\sigma_{\mathrm{CC}}}{r_{ij}}\right)^{12} - \left(\frac{\sigma_{\mathrm{CC}}}{r_{ij}}\right)^{6}\right], \quad (3)$$

excluding 1–2 and 1–3 C–C pairs. The parameters of the Lennard-Jones potential are obtained from the Universal Force Field (UFF) [27]. The carbon–water interaction is modeled as a carbon–oxygen Lennard-Jones potential with parameters $(\sigma_{\mathrm{CO}}, \epsilon_{\mathrm{CO}})$ obtained from Bojan and Steele [28]. Details and validation of the potentials are given elsewhere [18,19,29] and summarized in Table 1. The electrostatic interaction between carbon and water employed previously [18,30] was not used in the present study because its effect was found to be negligible in a series of validation studies [18].

The water molecules are initially placed on a rectangular lattice with spherical or cylindrical voids to accommodate the buckyballs and carbon nanotubes, respectively. During equilibration the temperature is adjusted to the desired value of 300 K using velocity scaling. For the fully periodic systems, the size of the

Table 1
Parameters for the carbon and water interaction potentials[a]

$K_{\mathrm{Cr}} = 478.9\ \mathrm{kJ\,mol^{-1}\,Å^{-2}}$	$r_{\mathrm{C}} = 1.418$ Å
$K_{\mathrm{C}\theta} = 562.2\ \mathrm{kJ\,mol^{-1}}$	$\theta_{\mathrm{C}} = 120.00°$
$K_{\mathrm{C}\phi} = 25.12\ \mathrm{kJ\,mol^{-1}}$[b]	$\gamma = 2.1867\ \mathrm{Å^{-1}}$
$\epsilon_{\mathrm{CC}} = 0.4396\ \mathrm{kJ\,mol^{-1}}$[c]	$\sigma_{\mathrm{CC}} = 3.851$ Å[c]
$\epsilon_{\mathrm{CO}} = 0.3126\ \mathrm{kJ\,mol^{-1}}$[b]	$\sigma_{\mathrm{CO}} = 3.19$ Å[b]

K_{Cr}, r_{C} and γ are the parameters of the Morse potential, $K_{\mathrm{C}\theta}$ and θ_{C} the angle parameters, and $K_{\mathrm{C}\phi}$, is the torsion parameter. ϵ_{CC} and σ_{CC} are the Lennard-Jones parameters for the carbon–carbon interaction.
[a] Ref. [25] unless otherwise indicated.
[b] Ref. [18].
[c] Ref. [27].

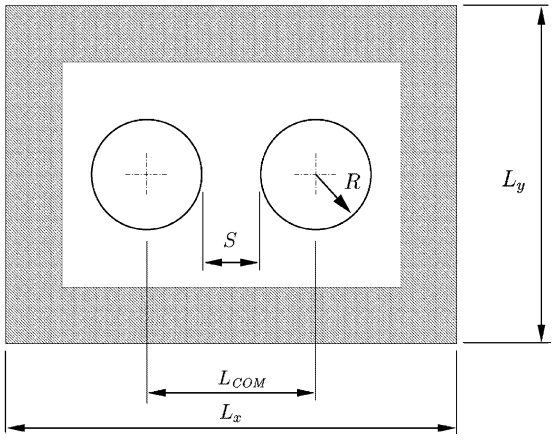

Fig. 1. Sketch of the C_{60} and carbon nanotube system. L_x and L_y denote the size of the system in the x and y direction, L_{COM} the center-of-mass spacing between the structures, and S the distance between the molecules. During the equilibration, the size of the computational box is adjusted to secure a bulk density of 997 $\mathrm{kg\,m^{-3}}$ in the bulk region (shaded area).

computational box is adjusted to match a bulk water density of 997 kg m^{-3}. The bulk properties are measured in the region excluding the C_{60} and CNT's and the interface regions that exhibit density variations cf. Fig. 1. No volume adjustment was performed for the systems with a free surface. These adjustments are switched off after the equilibration phase at 4 and 10 ps for the simulations of the CNT and C_{60}, respectively. For the fully periodic systems, the water–water electrostatic interactions are initially (during the first 0.2 ps) excluded to allow a faster filling of the interstices.

2.1. Constrained dynamics

To compute the potential of mean force (PMF) between the carbon nanotubes, separate simulations are conducted in which the distance between the center-of-mass (L_{COM}) of the CNT's is constrained cf. Fig. 1. The constraining force (F) is computed using a classical Proportional-Integral-Differential (PID) control algorithm [31]

$$F(t) = G\left(e + T_d \frac{de}{dt} + \frac{1}{T_i}\int_0^t e\,d\tau\right). \quad (4)$$

The force per carbon atom acts between the center-of-mass of the nanotubes to drive the difference (e) between the actual CNT spacing and the required value to zero. G is the gain of the controller, and T_d and T_i are the time constants of the P and I control, respectively. The constants are adjusted using the Ziegler–Nichols method [32] and values of $G = 16.2$ MJ mol^{-1} Å^{-2}, and $T_d = T_i = 31.4$ fs, are found to provide a fast, but well damped controller. The method is similar to the method of steered molecular dynamics [33] and traditional constrained dynamics [34], but provides an adaptive mechanism for computing the strength of the constraining potential for a given constraint. The algorithm furthermore allows dynamic adjustment of the (identical) initial configuration to match the desired spacing as demonstrated in Fig. 2. The main transient of the motion is completed in less than 0.5 ps and at equilibrium, the distance between the carbon nanotubes does not deviate more than 10^{-5} Å. Since the motion of the tubes at equilibrium is negligible, the statistical ensemble effectively remains microcanonical (the variation of the total energy is less than $\delta E_{tot}/E_{tot} < 0.02\%$ during the entire 0.1 ns simulation). Thus the potential of mean force can be computed directly from the constraining force as

$$\mathrm{PMF}(R) = \int_0^R F(r)\,dr, \quad (5)$$

where $F(r)$ is the time average of the constraining force [35–37].

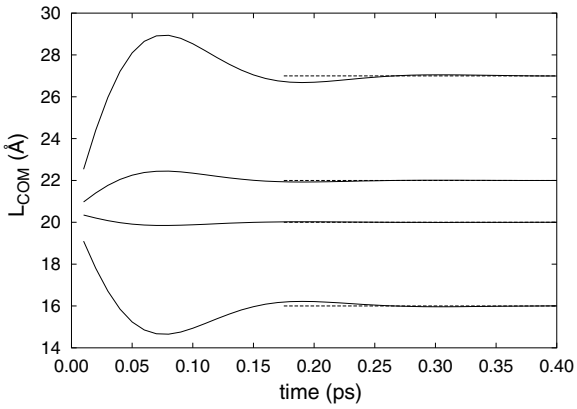

Fig. 2. Examples of the time history of the distance between the center-of-mass (L_{COM}) of the carbon nanotubes during equilibration for four different target spacings. The constraining force is computed using the Ziegler–Nichols method to allow a dynamic adjustment of the COM. —: transient of the L_{COM}; - - -: the target COM spacing.

3. Results

The C_{60} fullerene molecules are initially placed at a center-of-mass (COM) distance in the range 11.5–19.5 Å, which corresponds to a distance (S) between the molecules of 4.68–12.68 Å measured as the minimum distance between the carbon atoms on different fullerenes. The number of water molecules used in the simulations (cases 1–6) varies from 961 to 1020 for the small and large spacing, cf. Table 2. During the 15 ps equilibration, the COM spacing of the buckyballs is fixed to allow the water to fill the interstices between the buckyballs. Afterwards, the C_{60} molecules are released and allowed to move while the temperature and the volume adjustment are continued for another 10 ps. The simulations are continued for 160 ps or until drying occurs.

The simulations of unconstrained (16,0) carbon nanotubes in water (cases 7–12) involve 4536 water molecules and 2×832 carbon atoms, respectively. The two carbon nanotubes are placed with an initial spacing (S) in the range of 7.68–11.76 Å. The center-of-mass separation of the carbon nanotubes is constrained during a 4 ps equilibration period, after which they are released and free to move. However, the imposed periodic boundary condition will limit the motion and mainly allow an in-plane (x–y) motion. A rotation of the carbon nanotubes will result in an unfavourable stretching of the tubes. The simulations are continued for 100 ps or until the system reaches a drying state.

Finally, we consider a set of constrained simulations (cases 13–55) of carbon nanotubes in water to compute their potential of mean force. The simulations involve both a fully periodic system (cases 13–44), and simulations with a free surface of the water (cases 45–55), corresponding to carbon nanotubes immersed in a slab of water. Case 55 uses a purely repulsive Lennard-Jones

Table 2
Simulation cases for buckyballs (B), and carbon nanotubes (CNT) in water

Case	System	L_{COM} (Å)	S (Å)	N_w	N_c	t_m (ps)	r_c (Å)	Type
1	B	12.00	4.68	961	2×60	60	12.66	f
2	B	14.00	6.68	1018	2×60	60	12.66	f
3	B	15.00	7.68	1019	2×60	60	12.66	f
4	B	16.00	8.68	1123	2×60	85	12.66	f
5	B	18.00	10.68	1120	2×60	130	12.66	f
6	B	20.00	12.68	1120	2×60	130	12.66	f
7	CNT	20.51	7.68	4446	2×832	69	9.50	f
8	CNT	21.51	8.72	4446	2×832	60	11.10	f
9	CNT	22.51	9.95	4446	2×832	43	11.10	f
10	CNT	23.01	10.37	4446	2×832	64	11.10	f
11	CNT	23.51	10.94	4446	2×832	29	11.10	f
12	CNT	24.51	11.76	4446	2×832	100	11.10	f
13	CNT	15.50	2.98	4536	2×832	180	9.50	c
14	CNT	15.75	3.23	4536	2×832	180	9.50	c
15	CNT	16.00	3.48	4536	2×832	180	9.50	c
16	CNT	16.25	3.73	4536	2×832	180	9.50	c
17	CNT	16.50	3.97	4536	2×832	180	9.50	c
18	CNT	16.75	4.23	4536	2×832	180	9.50	c
19	CNT	17.00	4.47	4536	2×832	180	9.50	c
20	CNT	17.25	4.73	4536	2×832	180	9.50	c
21	CNT	17.50	4.98	4536	2×832	180	9.50	c
22	CNT	17.75	5.22	4536	2×832	180	9.50	c
23	CNT	18.00	5.48	4536	2×832	180	9.50	c
24	CNT	18.25	5.72	4536	2×832	180	9.50	c
25	CNT	18.50	5.98	4536	2×832	180	9.50	c
26	CNT	18.75	6.23	4536	2×832	180	9.50	c
27	CNT	19.00	6.47	4536	2×832	180	9.50	c
28	CNT	19.25	6.73	4536	2×832	180	9.50	c
29	CNT	19.50	6.97	4536	2×832	180	9.50	c
30	CNT	19.75	7.23	4536	2×832	180	9.50	c
31	CNT	20.00	7.48	4536	2×832	180	9.50	c
32	CNT	20.25	7.72	4536	2×832	180	9.50	c
33	CNT	20.50	7.98	4536	2×832	180	9.50	c
34	CNT	20.75	8.22	4536	2×832	180	9.50	c
35	CNT	21.00	8.48	4536	2×832	180	9.50	c
36	CNT	21.25	8.73	4536	2×832	180	9.50	c
37	CNT	21.50	8.97	4536	2×832	180	9.50	c
38	CNT	22.00	9.47	4536	2×832	180	9.50	c
39	CNT	22.50	9.98	4536	2×832	180	9.50	c
40	CNT	23.00	10.48	4536	2×832	180	9.50	c
41	CNT	24.00	11.47	4536	2×832	180	9.50	c
42	CNT	25.00	12.48	4536	2×832	180	9.50	c
43	CNT	26.00	13.48	4536	2×832	180	9.50	c
44	CNT	27.00	14.47	4536	2×832	180	9.50	c
45	CNT	16.00	3.47	4536	2×832	180	9.50	cs
46	CNT	17.00	4.47	4536	2×832	180	9.50	cs
47	CNT	18.00	5.47	4536	2×832	180	9.50	cs
48	CNT	19.00	6.47	4536	2×832	180	9.50	cs
49	CNT	20.00	7.47	4536	2×832	180	9.50	cs
50	CNT	21.00	8.47	4536	2×832	180	9.50	cs
51	CNT	22.00	9.47	4536	2×832	180	9.50	cs
52	CNT	23.00	10.47	4536	2×832	180	9.50	cs
53	CNT	24.00	11.47	4536	2×832	180	9.50	cs
54	CNT	25.00	12.47	4536	2×832	180	9.50	cs
55	CNT	27.00	14.47	4536	2×832	180	9.50	cs
56	CNT	–	–	12,402	16×832	135	9.50	f

The simulations allow the buckyballs and carbon nanotubes to move freely (f) during the simulation, or constrained (c) subject to periodic boundary conditions or constrained within a slab of water (cs). L_{COM} denotes the initial center-of-mass separation of the nanotubes, S the minimal initial tube distance, and N_w, N_c, t_m, and r_c the number of water molecules, the number of carbon atoms, the simulation time and the cutoff radius, respectively. For the (f) cases, S is measured after the initial equilibration with fixed L_{COM}. Case 55 is run with a purely repulsive potential, cf. text.

between the carbon and oxygen atoms to study the effect of a strongly hydrophobic interface. The simulations are carried out for 180 ps and the statistics are collected after 120 ps when the individual components of the potential energy have converged to stable values.

3.1. Buckyballs in water

For the simulations of buckyballs in water, we find that the systems with an initial spacing S less than 12 Å exhibit drying that results in a direct contact between the buckyballs as shown in Fig. 3, whereas a larger initial spacing results in a continuous wetting. Snapshots of the systems corresponding to the drying and wetting states are shown in Fig. 4. The separation at which the transition occurs allows approximately two layers of interstitial water molecules which, depending on the relative orientation of the fullerenes, is between 8.5 and 9.6 Å for a staggered and inline arrangement of the carbon–oxygen atoms (C–O–O–C), respectively. A similar threshold value was found by Wallqvist and Berne [38] for water confined between structureless hydrophobic surfaces. In the present study the interstitial water is observed to be subject to an occasional compression due to the fluctuations of the position of the C_{60} molecules. This compression leads to a decrease in S and finally destabilizes the interstitial water layer as demonstrated by the 16 and 18 Å cases shown in Fig. 3. The expulsion of the interstitial water proceeds in two steps (see Fig. 3): first the thickness of the water layer is reduced to a single metastable layer of water molecules with a thickness of 5.7–6.4 Å and a lifetime under 40 ps and then this single layer of water is expelled in 5–10 ps. The systems which exhibit a drying behavior all reach their van der Waals equilibrium at a carbon–carbon distance of 3.2 Å.

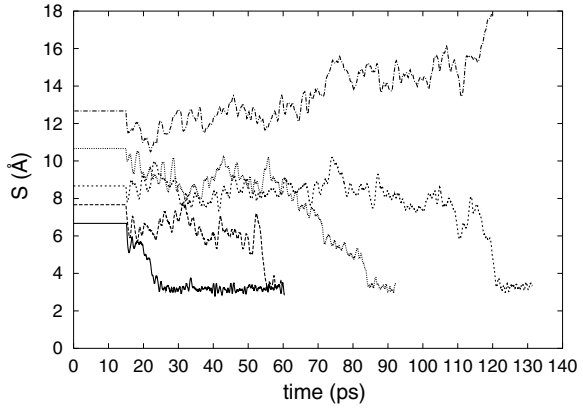

Fig. 3. Time history of the minimum carbon–carbon spacings (S) between two buckyballs in water for different initial center-of-mass spacing: —: 14 Å; ——: 15 Å; – – –: 16 Å; - - -: 18 Å; – – –: 20 Å.

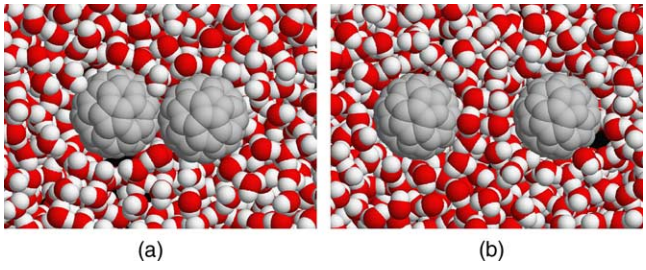

Fig. 4. Snapshots from the simulations of buckyballs in water. An initial center-of-mass spacing of 14 Å results in a drying of the interface (a), whereas buckyballs placed at a distance beyond 20 Å exhibit a continued wetting (b).

3.2. Carbon nanotubes in water

A similar behavior is observed for a parallel pair of unconstrained carbon nanotubes in water as shown in Fig. 5. The critical spacing dividing the drying and the wetting state is approximately 12 Å similar to the threshold value found for the buckyballs in water. The drying of the carbon nanotubes generally proceeds in three steps: a first metastable configuration is reached at a separation of 7.5–8.5 Å (Fig. 5) which is approximately 1 Å less than the spacing required to support two layers of water molecules. This reduced value is caused by the compression of the interstitial water molecules. Next, a distinct plateau is reached for one layer of interstitial waters at $S = 5.5$–5.8 Å with a lifetime up to 30–40 ps. Finally, a complete drying state is reached at the equilibrium spacing of 3.5 Å. The actual transitions between the metastable separation and the dry state occur rapidly over a time of 1–3 ps.

3.3. Potential of mean force

Constrained molecular dynamics simulations have been performed for the two carbon nanotubes in water (cases: 13–55) to extract the potential of mean force (PMF) governing the drying transition. The simulations

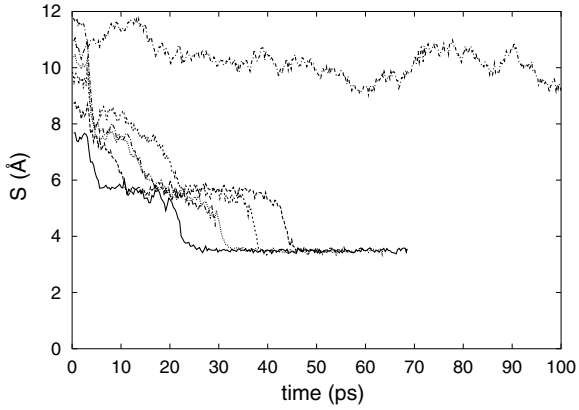

Fig. 5. The time history of the minimum carbon–carbon spacing (S) between two carbon nanotubes in water. The initial center-of-mass spacings are: —: 12 Å; – – –: 14 Å; · · ·: 16 Å; - - -: 17 Å; - -·- -: 18 Å; – – –: 20 Å.

involve both a fully periodic system (cases: 13–44) and a slab with a pair of free surfaces (cases: 45–55) to study the effect of the finite size system imposed by the periodic boundary conditions. For large system sizes the two are equivalent, whereas the fully periodic system may force or prevent drying for small system sizes.

At equilibrium, the constraining force (F) balances the hydration force ($F = -F_{\mathrm{hyd}}$) which allows us to compute the corresponding potential of mean force (Eq. (5)). The constraining force and the PMF per unit length of the carbon nanotube are shown in Fig. 6 and snapshots from the simulations are shown in Fig. 7. Both the simulations using full and partial periodic boundary conditions display a qualitatively similar drying transition as demonstrated in the constraining force and PMF shown in Fig. 6. The first equilibrium configuration is found at the point of van der Waals contact at a separation of approximately 3.2 Å. At shorter spacings, the constraining force is negative due to van der Waals repulsion of the nanotubes. The attractive part of the force reaches its maximum at a tube spacing of 5.0 Å (see Figs. 6a and 7b) which is approximately 1 Å less than the spacing required to host one layer of water. The main difference between the simulations using different boundary conditions is found at a tube spacing of 5.24 Å (0.24 Å beyond the maximum) where the slab system displays a weaker force ($\approx$6.0 kJ mol^{-1} Å^{-2}) compared to the fully periodic system ($\approx$8.1 kJ mol^{-1} Å^{-2}). After the maximum is reached the force decreases rapidly at larger distances and reaches a low, but positive value at a tube spacing of 6–7 Å which allows accommodation of one unstable layer of water. Finally, a weak depression in the force is observed at a spacing of 9–10 Å corresponding to a metastable interstitial region with two layers of waters. The use of constrained dynamics eliminates the compression of the interstitial water layer found in the studies of the unconstrained fullerenes, and thereby enhances the stability of the two-layer configuration. For the 12.5 Å diameter carbon nanotubes considered in the the present study, the magnitude of the PMF per unit length is ≈ -17 kJ mol^{-1} Å^{-1} (Fig. 6b), which is in reasonable agreement with the analysis of Lum et al. [39] of water interacting with four parallel hard cylinders. Their analysis results in values of the PMF of −12 and −23 kJ mol^{-1} Å^{-1} for cylinders with a radius of 5 and 6 Å, respectively. However, the present study indicates that the main contribution to the PMF is the van der Waals attraction between the carbon nanotubes as demonstrated by measuring the force between two rigid carbon nanotubes in vacuum (Fig. 6a). The deformation of the carbon nanotubes allowed by the simulations of carbon nanotubes in water reduces the maximum attraction between the tubes and the point of the maximum attraction occurs at a larger separation.

The snapshots shown in Fig. 7c–e reveal an interstitial vapor phase indicative of cavitation [39–43] for the

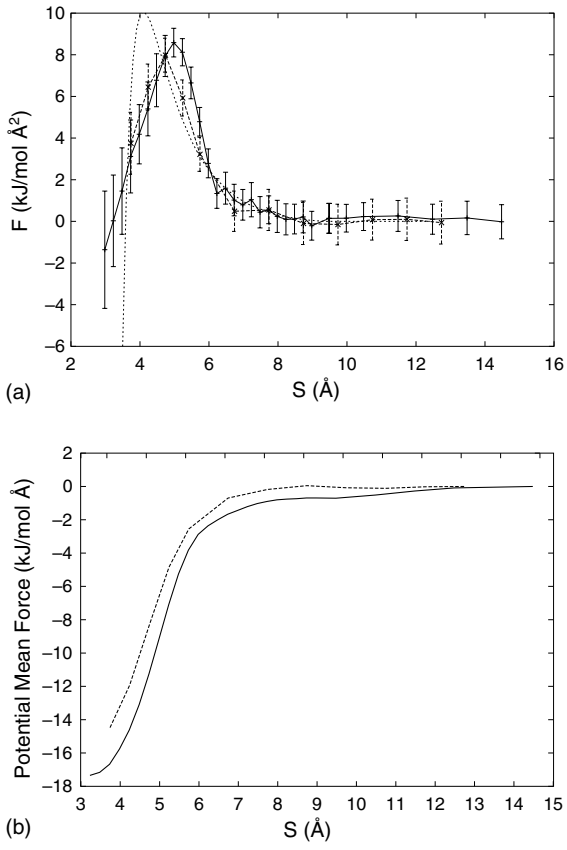

Fig. 6. Constraining force per unit length of the carbon nanotube (a) for the periodic system (—), for a slab system (– –), and for rigid carbon nanotubes in vacuum (···). The corresponding potential of mean force per unit length of the carbon nanotube is shown in (b). The reaction coordinate is the tube spacing (S). The potential is arbitrarily set to zero at the maximum tube spacing. The error bars (a) indicate the standard deviation of the constraining force.

metastable pre-drying state and an apparently stable water layer at larger tube spacing (cf. Fig. 7f). A similar vapor phase is found in the simulations using a slab as shown in Fig. 8. The snapshots (a) and (b) correspond to the cases shown in Fig. 7b and e. A density profile across the interstitial region is shown in Fig. 9 for the three cases (29, 38, and 44), with $S = 6.98$, 9.48, and 14.48 Å, corresponding to Fig. 7c, e, f, respectively. The interstitial density exhibits the characteristic profile of water at a hydrophobic surface with density peaks of $\approx$2000 kg m^{-3} and a superposition of the second peaks in the interstitial region for the $S = 14.48$ Å case. At lower tube spacings, the interstitial density is reduced to values of 500 and 200 kg m^{-3}, respectively. This relatively short range of the hydrophobic interaction is in accord with recent experiments [44], where pure hydrophobic surfaces were found to have a short range hydrophobic attraction with an estimated range less than 15–20 nm [45,46] and possibly even shorter [45]. Though the present interface is strongly hydrophobic (contact angle exceeding 90°) we furthermore considered a purely

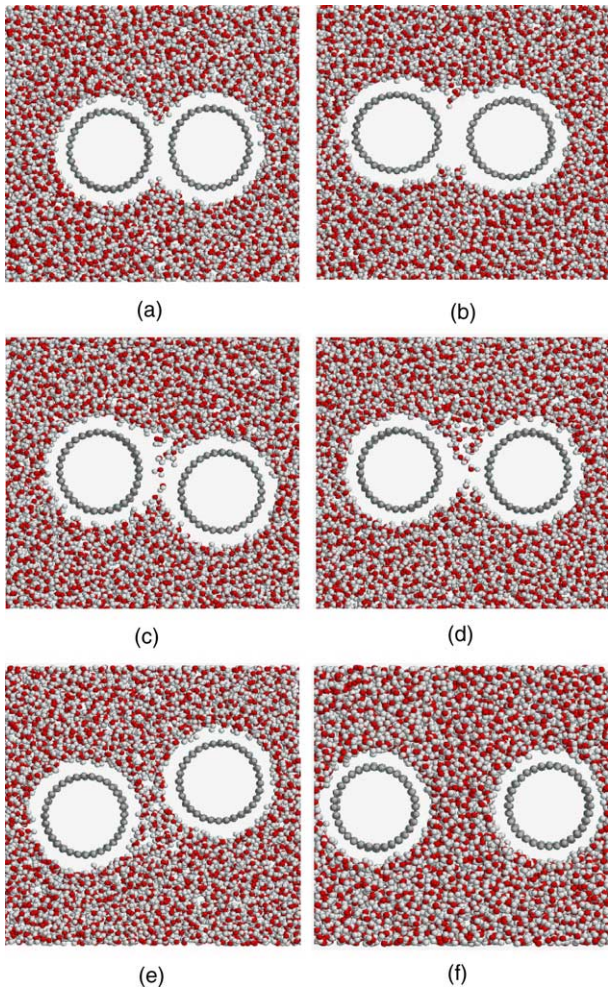

Fig. 7. Snapshot of the atoms for the simulation of two carbon nanotubes in water (cases: 15, 23, 29, 33, 38, and 44). The views are closeups; the dimension of the system is 70×44×60 Å. The center-of-mass distance and the minimum carbon–carbon spacing in parenthesis is 16.0 (3.48), 18.0 (5.48), 19.5 (6.98), 20.5 (7.98), 22.0 (9.48), and 27.0 (14.48) Å respectively.

repulsively carbon water interaction $U(r) = 4\epsilon_{CO} \times (\sigma_{CO}/r_{(ij)})^{12}$ corresponding to a contact angle of 180°. At these conditions a "long-range" hydration is observed cf. Fig. 8c ($S = 14.47$ Å). However, we emphasize that this interaction potential is artificial and using realistic parameters results in a very weak hydration.

3.4. Energetics of hydration

From the analysis of the individual components of the potential energy during the constrained dynamics, we can gain insight into the drying process. At $S = 9.0$–9.5 Å, corresponding to the metastable two-layer interstitial water condition (Fig. 7e), the average water Coulomb and Lennard-Jones (LJ) energies exhibit a small minimum and maximum, respectively, relative to larger separations. At $S = 8$ Å, where half of the interstitial water has been expelled (Fig. 7d), the water Coulomb and LJ energies exhibit a maximum and a minimum, respectively, and the carbon valence energy is at a maximum. Here the deformation of the nanotubes is the greatest, but the mean force between them is only slightly higher than the asymptotic value. After the interstitial water has been expelled ($S \approx 6$ Å) there is a sizable increase in the mean force and the water Coulomb energy is considerably lower while the water LJ energy is at a maximum. The water energies probably are indicative of compression of the water molecules near the surface of the hydrophobic cavity. As seen in Fig. 9, the water density spike is higher for the drying case. At this point there is also a lowering of the carbon LJ energy as the van der Waals attraction between the nanotubes is activated. The expulsion of the interstitial water clearly occurs before the nanotubes are pulled together. Overall, the PMF (Fig. 6b) most closely resembles the average carbon LJ energy term. For the drying of nanotubes illustrated in Fig. 5, lowering of the carbon LJ energy correlates strongly with the decrease in S. However, in these cases, interstitial water layers persist at smaller separations than in the constrained MD. For example, the cases at $S = 8$ and 6 Å, correspond to two and one interstitial water layers, respectively. Also, lowering of the carbon LJ energy is more noticeable before the interstitial water is expelled.

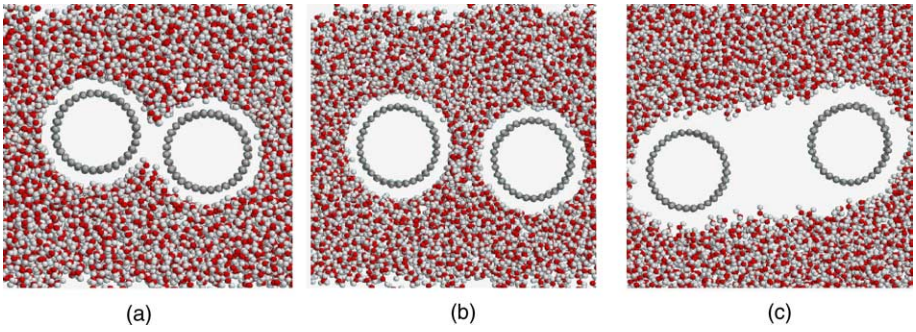

Fig. 8. Snapshots of the simulations of two carbon nanotubes in a slab of water at center-of-mass distances of 18.0 Å (case 47), 22.0 Å (case 51), and 27.0 Å (case 55), respectively. The views are closeups; the dimensions of the system are $70 \times \infty \times 60$ Å. The free surfaces of the slab are at the top and bottom of the snapshots. Note that in (c), a purely repulsive water-carbon potential is applied, cf. text.

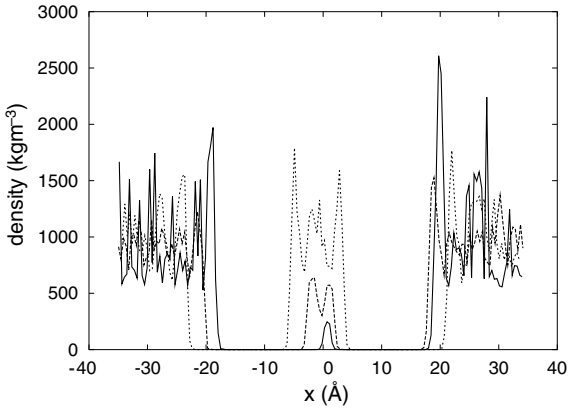

Fig. 9. The water density profile through the interstitial region for different tube spacings (S): —: 6.98 Å (case 29), – – –: 9.48 Å (case 38), and - - -: 14.48 Å (case 44).

3.5. Hydration of arrays of carbon nanotubes

Although the range of the hydrophobic interaction is found to be moderate, its overall effect is thought to play a vital role in the self-organization and assembly of molecular structures such as membrane and nanoscale structures and for the folding of DNA [47–49]. For example, hydrophobic interactions were found to destabilize arrays of carbon nanotubes considered for biosensing and resulting in a drying and clustering of the system [5].

To demonstrate the collective effect of hydrophobic hydration for these systems we consider 16 unconstrained (16,0) carbon nanotubes in water (case 56) as shown Fig. 10. The system consists of 16×832 carbon atoms and 12,402 water molecules. The tubes are initially placed in a four by four arrangement with an initial center-of-mass distance of 20 Å corresponding to a spacing between the tubes of 7.48 Å which allows a single layer of interstitial waters (Fig. 10a). The individual center-of-mass of the carbon nanotubes are fixed during a 4 ps equilibration period after which they are released. During the first 12 ps after release drying is observed between pairs of carbon nanotubes that move into contact. In a second phase, pairs of one and two carbon nanotubes come into contact mainly by the motion of the single carbon nanotubes (Fig. 10e and f). After 40 ps, two groups of three and seven carbon nanotubes form a closed ring with a pocket of trapped water due to the enforced periodicity of the simulation. At longer times, other groups of tubes join this ring and encapsulate water molecules in the interstices. In a non-periodic system the trapped water molecules would be more easily expelled. This demonstrates the tendency of carbon nanotubes to form insoluble bundles (or ropes) in aqueous solutions as observed in Ref. [5]. Clearly a suspension of individual carbon nanotubes in water would form a "precipitate" of carbon nanotube ropes, exemplifying the insolubility of carbon nanotubes in water.

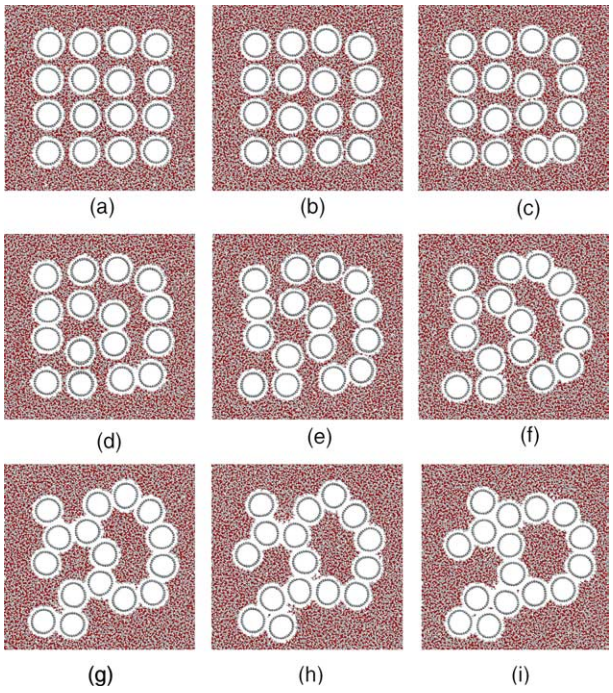

Fig. 10. Snapshot from the simulation of 16 carbon nanotubes in water (a–i: 4, 8, 10, 12, 16, 20, 40, 80, and 120 ps). From an initial regular four by four arrangement (a) the system evolves into a bundle of closely packed tubes with occasionally trapped water pockets. The periodicity of the system prevents these pockets to empty.

4. Summary and conclusions

The hydrophobic–hydrophilic behavior of C_{60} fullerene molecules and carbon nanotubes in water has been studied using molecular dynamics simulations. The results indicate a drying behavior of the interstices for an initial spacing between the fullerenes less than 12 Å, and 9–10 Å for the carbon nanotubes, respectively, corresponding to the thickness of two layers of water molecules. Applying a classical PID control algorithm to constrain the dynamics of the center-of-mass of the carbon nanotubes we derive the potential of mean force governing the drying process of two (16,0) carbon nanotubes in water. We find that the constraining force displays a maximum at a tube spacing of 5.0 Å corresponding to one layer of unstable interstitial waters. To study the effect of finite system size imposed by the periodic boundary conditions we furthermore conduct simulations of carbon nanotubes immersed in a slab of water. The potential of mean force for this system is in qualitative agreement with the periodic system, hence indicating that the size of the periodic system is sufficiently large to mimic an infinite system. Comparing the

hydration force with the force acting between the carbon nanotubes in vacuum indicates that the hydration is dominated by the van der Waals forces between the carbon nanotubes. Finally, we have conducted an initial study of the drying process of bundles of (16,0) carbon nanotubes in water. From an initial spacing of 20×20 Å arranged in a Cartesian array of four by four the system undergoes a drying transition forming carbon nanotube ropes. The insolubility of carbon nanotubes in water is manifested by this rope formation. The waters initially trapped in the interstitial regions remain trapped throughout the simulation due to the imposed periodic boundary conditions. Further studies are currently being conducted using finite-length tubes.

Acknowledgements

We wish to acknowledge discussions with Andrew Pohorille and Christopher Dateo at NASA Ames Research Center, and with Flavio Noca at Jet Propulsion Laboratory.

Support for TH is provided by NASA contract NAS2-99092 to ELORET Corporation. Support from the Research Commission at ETH Zürich, and from the CTR Summer Programs 2000/2002 Stanford University are greatly appreciated.

References

[1] Jarvis SP, Uchihashi T, Ishida T, Tokumoto H, Nakayama Y. Local solvation shell measurement in water using a carbon nanotube probe. J Phys Chem B 2000;104(26):6091–4.

[2] Moloni K, Buss MR, Andres RP. Tapping mode scaling force microscopy in water using a carbon nanotube probe. Ultramicroscopy 1999;80:237–46.

[3] Li J, Cassell AM, Dai H. Carbon nanotubes as AFM tips: measuring DNA molecules at the liquid/solid interface. Surf Interface Anal 1999;28:8–11.

[4] Balavoine F, Schultz P, Richard C, Mallouh V, Ebbesen TW, Mioskowski C. Helical crystallization of proteins on carbon nanotubes: a first step towards the development of new biosensors. Angew Chem 1999;38(13/14):1912–5.

[5] Nguyen CV, Delzeit L, Cassell AM, Li J, Han J, Meyyapan M. Preparation for nucleic acid functionalized carbon nanotube arrays. Nano Lett 2002;2(10):1079–81.

[6] Boyd GE, Livingston HK. Adsorption and the energy changes at crystalline solid surfaces. J Am Chem Soc 1942;64:2383–8.

[7] Young GJ, Chessick JJ, Healey FH, Zettlemoyer AC. Thermodynamics of the adsorption of water on graphite from heats on immersion and adsorption data. J Phys Chem 1954;58:313–5.

[8] Müller EA, Rull LF, Vega LF, Gubbins KE. Adsorption of water on activated carbons: a molecular simulation study. J Phys Chem 1996;100(4):1189–96.

[9] Adamson AW, Gast AP. Physical chemistry of surfaces. 6th ed. New York: John Wiley & Sons; 1997.

[10] Hamon MA, Chen J, Hu H, Chen Y, Itkis MA, Rao AM, et al. Dissolution of single-walled carbon nanotubes. Adv Mater 1999;11(10):834–40.

[11] Bahr JL, Mickelson ET, Bronikowski MJ, Smalley RE, Tour JM. Dissolution of small diameter single-wall carbon nanotubes in organic solvents? Chem Commun 2001;2:193–4.

[12] Ausman KD, Piner R, Lourie O, Ruoff R, Korbov M. Organic solvent dispersions of single-walled carbon nanotubes: toward solutions of pristine nanotubes. J Phys Chem B 2000;104(38):8911–5.

[13] Ruoff RS, Tse DS, Malhotra R, Lorents DC. Solubility of C_{60} in a variety of solvents. J Phys Chem 1993;97:3379–83.

[14] Chen J, Hamon MA, Hu H, Chen Y, Rao AM, Eklund PC, et al. Solution properties of single-walled carbon nanotubes. Science 1998;282:95–8.

[15] Dujardin E, Ebbesen TW, Krishnan A, Treacy MMJ. Wetting of single shell carbon nanotubes. Adv Mater 1998;10(17):1472–5.

[16] Gogotsi Y, Libera JA, Güvenç-Yazicioglu A, Megaridis CM. In situ multiphase fluid experiments in hydrothermal carbon nanotubes. Appl Phys Lett 2001;79(7):1021–3.

[17] Gogotsi Y, Naguib N, Libera JA. In situ chemical experiments in carbon nanotubes. Chem Phys Lett 2002;365:354–60.

[18] Walther JH, Jaffe R, Halicioglu T, Koumoutsakos P. Carbon nanotubes in water: structural characteristics and energetics. J Phys Chem B 2001;105:9980–7.

[19] Werder T, Walther JH, Jaffe R, Halicioglu T, Noca F, Koumoutsakos P. Molecular dynamics simulations of contact angles of water droplets in carbon nanotubes. Nano Lett 2001;1(12):697–702.

[20] Hummer G, Rasaiah JC, Noworyta JP. Water conduction through the hydrophobic channel of a carbon nanotube. Nature 2001;414:188–90.

[21] Noon WH, Ausman KD, Smalley RE, Ma J. Helical ice-sheets inside carbon nanotubes in the physiological condition. Chem Phys Lett 2002;355:445–8.

[22] Koga K, Gao GT, Tanaka H, Zeng XC. Formation of ordered ice nanotubes inside carbon nanotubes. Nature 2001;412:802–5.

[23] Teleman O, Jönsson B, Engström S. A molecular dynamics simulation of a water model with intramolecular degrees of freedom. Mol Phys 1987;60(1):193–203.

[24] Levitt M, Hirshberg M, Sharon R, Daggett V. Potential energy function and parameters for simulations of the molecular dynamics of proteins and nucleic acids in solutions. Comput Phys Commun 1995;91:215–31.

[25] Guo Y, Karasawa N, Goddard III WA. Prediction of fullerene packing in C_{60} and C_{70} crystals. Nature 1991;351:464–7.

[26] Tuzun RE, Noid DW, Sumpter BG, Merkle RC. Dynamics of fluid flow inside carbon nanotubes. Nanotechnology 1996;7(3):241–8.

[27] Rappé AK, Casewit CJ, Colwell KS, Goddard III WA, Skiff WM. UFF, a full periodic table force field for molecular mechanics and molecular dynamics simulations. J Am Chem Soc 1992;114:10024–35.

[28] Bojan MJ, Steele WA. Interactions of diatomic molecules with graphite. Langmuir 1987;3(6):1123–7.

[29] Kotsalis EM, Jaffe RL, Walther JH, Werder T, Koumoutsakos P. Buckyballs in water: structural characteristics and energetics. Annual research briefs, Center for Turbulence Research, Stanford, 2001.

[30] Marković N, Andersson PU, Någård MB, Petterson JBC. Scattering of water from graphite: simulations and experiments. Chem Phys 1999;247:413–30.

[31] Åström KJ, Hägglund T. PID controllers: theory, design, and tuning. 2nd ed. Research Triangle Park, NC: Instrument Society of America; 1995.

[32] Ziegler JG, Nichols NB. Optimum settings for automatic controllers. J Dyn Syst—T ASME 1993;115(2B):220–2.

[33] Izrailev S, Stepaniants S, Isralewitz B, Kosztin D, Lu H, Molnar F, et al. Steered molecular dynamics. Lecture notes in computational science and engineering 1998;4:36.

[34] van Gunsteren WF, Berendsen HJC. Algorithms for macromolecular dynamics and constraint dynamics. Mol Phys 1977; 37(5):1311–27.
[35] Straatsma TP, Zacharias M, McCammon JA. Holonomic constraint contributions to free energy differences from thermodynamic integration molecular dynamics simulations. Chem Phys Lett 1992;196(3/4):297–302.
[36] Mülders T, Krüger P, Swegat W, Schlitter J. Free energy as the potential of mean constraint force. J Chem Phys 1996;104(12): 4869–70.
[37] den Otter WK, Briels WJ. The calculation of free-energy differences by constrained molecular-dynamics simulations. J Chem Phys 1998;109(11):4139–46.
[38] Wallqvist A, Berne BJ. Computer simulation of hydrophobic hydration forces on stacked plates at short range. J Phys Chem 1995;99:2893–9.
[39] Lum K, Chandler D, Weeks JD. Hydrophobicity at small and large length scales. J Phys Chem B 1999;103:4570–7.
[40] Derjaguin BV, Churaev NV. Structural components of disjoining pressure. J Coll Interface Sci 1974;49:249–55.
[41] Christenson HK, Claesson PM. Cavitation and the interaction between macroscopic hydrophobic surfaces. Science 1988;239: 390–2.
[42] Attard P. Bridging bubbles between hydrophobic surfaces. Langmuir 1996;12:1693–5.
[43] Ederth T. Substrate and solution effects on the long-range "hydrophobic" interaction between hydrophobized gold surfaces. J Phys Chem B 2000;104:9704–12.
[44] Ishida N, Inoue T, Miyahara M, Higashitani K. Nano bubbles on a hydrophobic surface in water observed by tapping-mode atomic force microscopy. Langmuir 2000;16:6377–80.
[45] Hato M. Attractive force between surfaces of controlled "hydrophobicity" across water: a possible range of "hydrophobic interactions" between macroscopic hydrophobic surfaces across water. J Phys Chem 1996;100:18530–8.
[46] Carambassis A, Jonker LC, Attard P, Rutland MW. Forces measured between hydrophobic surfaces due to a submicroscopic bridging bubble. Phys Rev Lett 1998;80(24):5357–60.
[47] Makhatadze GI, Privalov PL. Contribution of hydration to protein folding thermodynamics. J Mol Biol 1993;232(2):639–59.
[48] Spolar RS, Record Jr MT. Coupling of local folding to site-specific binding of protein to DNA. Science 1994;263:777–84.
[49] Schwabe JWR. The role of water in protein–DNA interactions. Curr Opin Struct Biol 1997;7:126–34.